Chemical Engineering Journal 427 (2022) 132046

Contents lists available at ScienceDirect

Chemical Engineering Journal

journal homepage: www.elsevier.com/locate/cej

Designing advanced 0D-2D hierarchical structure for Epoxy resin to accomplish exceeding thermal management and safety

Jingyi Lu, Bibo Wang *, Pengfei Jia, Wenhua Cheng, Can Liao, Zhoumei Xu, Liang Cheng, Yuan Hu *

State Key Laboratory of Fire Science, University of Science and Technology of China, 96 Jinzhai Road, Hefei, Anhui 230026, People's Republic of China

ARTICLE INFO

Keywords:
Hierarchical structure
Thermal management
MXene
Fire safety
Toxicity suppression

ABSTRACT

Epoxy resin (EP) is widely used in the package of modern electronic products for thermal management, but the extremely flammability and toxicity release have restricted its further application. In this article, zinc hydroxystannate (ZHS) nanocubes were *in-situ* fabricated on the surface of titanium carbide ($Ti_3C_2T_x$) MXene nanosheets (ZHS@M) for improving the thermal management capacity of EP. Due to the phonon thermal conductance from ZHS and electron-hole thermal conductance of $Ti_3C_2T_x$, the thermal conductivity was improved by 328% compared with the neat EP, which was benefit to dissipate heat for reducing the possibility of thermal disaster chain happening. Furthermore, owing to the 0D-2D hierarchical structure of ZHS@M, the fire safety and smoke suppression of these EP composites were highly strengthened. The peak heat release rate (pHRR) and total heat release (THR) decreased by 54.91% and 58.74%, respectively. Moreover, hazardous gases of EP during the combustion were also efficiently reduced, and the generation of carbon oxide (CO) and carbon dioxide (CO_2) were decreased by 44.44% and 39.46% when the additive of ZHS@M was only 2 wt%. As a result, ternary catalytic effect and labyrinth structure improved the safety of EP in the thermal runaway incidents. Besides, EP-2.0 ZHS@M exhibited excellent tensile robustness (64.71 MPa) and modulus (2.39 GPa), which regarded as a reliable supporting material for electronics in thermal management field. Hence, this hierarchical EP-ZHS@M composites provided the help of cleaning the thermal accumulation and increasing fire safety while facing thermal runaway, which was significant to destroy the formation of thermal disaster chain and further applications of the modern electrons and devices.

1. Introduction

With increasing development of scientific technology, the modern industry has obtained a meteoritic progress in our daily lives[1,2]. In particular, the advances of modern electronic products have been paid more and more attentions, which highly promoted the operation of society and civilization. Unfortunately, the large usage of electronic products raises uncountable heat, which is unavoidable and leading to heat pollution[3,4]. Moreover, this heat easily develops into thermal runaway and finally triggers fire risk, resulting the loss of wealth and danger of human life. Even badly, the polymeric materials, flammable and hazardous when facing heat, are commonly used in the package for modern electronic products, leading a fire when the thermal runaway occurred[5,6]. Therefore, it is a vital to create an efficient and promising approach to take over this drawback and enhance the thermal management capacity of these package polymeric materials.

Typically, preparing composites is one of the most efficient and facile approach for enhancing the thermal management capacity of the electronic package materials. Introducing inorganic nanomaterials into polymer matrix is a widely used strategy to improve not only thermal conductivity but also fire safety of these polymeric materials[4]. In addition, inorganic nanomaterials can not only enhance the fire retardancy but also significantly enhance smoke suppression effect of polymers. Epoxy resin (EP) is one of the most important thermosetting advanced polymers in the electronic fields due to high tensile property, high adhesion to substrates, and good chemical and corrosion resistance. However, the low thermal conductivity (~0.2 W/m·K) has limited its further applications in the modern electronics, especially in the heat radiation field[7]. Apparently, this shortcoming is not benefit to be a promising thermal management material for the electronic products. Furthermore, under the situation of thermal runaway, EP is extremely flammable, and toxicity release during combusting, which is considered

* Corresponding authors.
E-mail addresses: wbibo@ustc.edu.cn (B. Wang), yuanhu@ustc.edu.cn (Y. Hu).

https://doi.org/10.1016/j.cej.2021.132046
Received 22 June 2021; Received in revised form 7 August 2021; Accepted 21 August 2021
Available online 26 August 2021

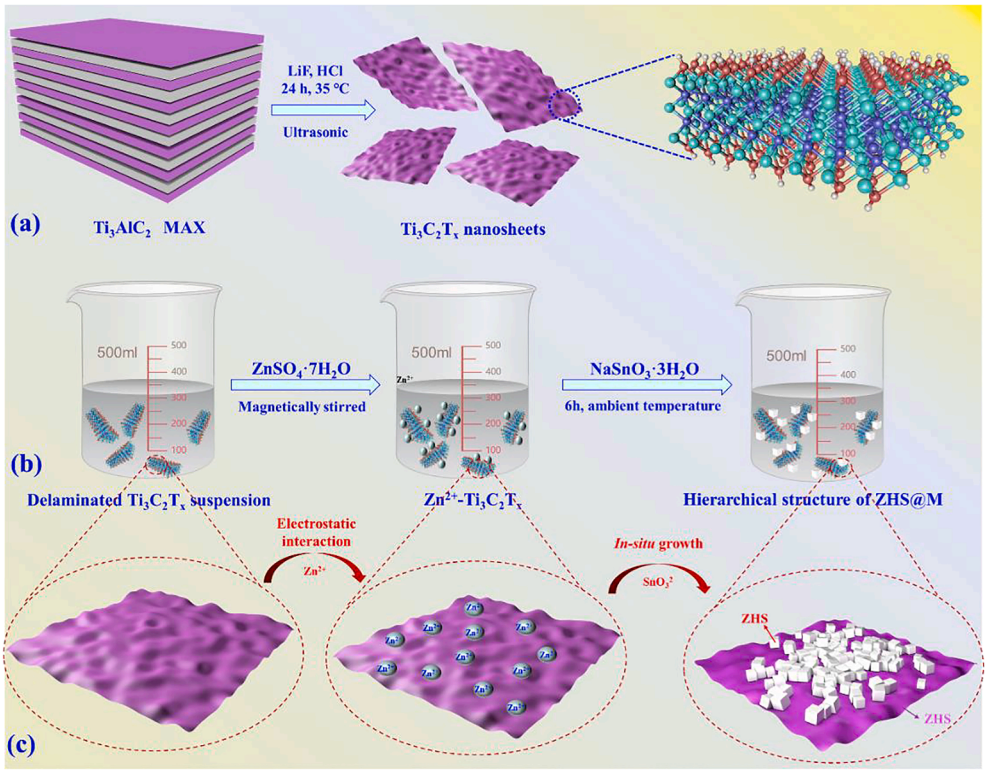

Fig. 1. (a) Preparation of 2D $Ti_3C_2T_x$ MXene; (b) synthetic scheme of ZHS@M; (c) details of the formation of hierarchical 0D-2D structure ZHS@M.

toxic and harmful for human health, under long-term application in the electronics or devices. Therefore, it is a vital to enhance its fire safety to meet the demand for the developing modern electronic products. In general, preparing flame-retardant EP composites have been considered as the facile and efficient approach via using flame retardancy. Besides, in order to fulfill the requirements of high efficiency flame retardance and environment-friendly principles, adding halogen-free FRs into EP has attracted increasing extensive attention.

Now, many types of nanomaterials such as graphene, phosphorene, layered double hydroxides (LDH), and transition metal dichalcogenides (TMDs) have been applied to decorate polymers[8–10]. In other words, two-dimensional (2D) nanomaterials are considered as one of the promising nano-flame retardants in preparing fire safe polymer composites. Besides, the large specific area and transition metallic atom offer superior barrier effect and catalytic capacity for the toxic gases, respectively. And the electron-hole obviously provide promising thermal conductance for the polymer composites[11].

Recently, MXene have been firstly synthesized from MAX phase by Yury Gogosti's group [12]. There are a great number of reports about the applications of MXene, such as supercapacitors, lithium-ion battery, electrochemical catalysis and so on. Typically, MXene was prepared by selectively etching $M_{n+1}AX_n$ phase, where M means the transition-metal elements, A refers to a group of IIIA or IVA element, X is C, N, and n = 1, 2, 3. $Ti_3C_2T_x$, a typical member of MXene family, was commonly used in many applications. The exceptional intrinsic specific area and abundant transition metallic atoms indicated the MXene had a powerful potential applied in preparing fire safe materials. More importantly, the rich content of surface groups of $Ti_3C_2T_x$ (–OH, =O, —F) offers the great potential and convenience to construct MXene-based hierarchical structure nanomaterials[12–14].

In addition, zinc hydroxystannate (ZHS) has caught extensive attention owing to it excellent catalytic capacity, thus significantly improving flame retardancy and smoke suppression ability of polymers [15,16]. Moreover, synergistic effect among different nanofillers may endow polymer composites with other unique functions beyond flame retardancy. The bio-mimetic hierarchical structure encourages different performance at a same time and exhibits extraordinary synergistic performance in the flame retardant field[17]. Besides, because of the high crystalline behavior of ZHS, the phonon delivery is extremely to be accomplished, which demonstrated the enhancement of thermal conductance in the ZHS@polymer composites. Notedly, the much electron-hole pair from $Ti_3C_2T_x$ is also benefit to improve the thermal management capacity of the polymer composites.

Hence, according to the above discussion, there were a design of 0D-2D hierarchical structure of ZHS@$Ti_3C_2T_x$ (ZHS@M) fabricating for enhancing thermal management capacity and the safety of epoxy resin when facing thermal runaway situation. The structures and morphology of ZHS@M and EP composites were systematically investigated by TEM, XPS, XRD and SEM. Furthermore, thermal conductivity was adopted to investigated the thermal management behavior of these EP-ZHS@M composites. And TGA results illustrated that the incorporation of ZHS@M shows a higher char residue compared with the addition of $Ti_3C_2T_x$ or ZHS separately. Most essentially, EP-ZHS@M composites exhibited increasing flame retardancy and the smoke suppression capacity was evaluated by cone calorimeter test and TG-IR, and the flame retardant mechanism was systematically studied. In addition, ZHS@M effectively decreased the permeation of pyrolysis hazardous compounds (PHCs) and fire hazard in the thermal runaway incident, which provided a meaningful method for strengthening the management in thermal disaster of modern electronic products.

2. Experimental sections

2.1. Materials

Zinc sulfate heptahydrate ($ZnSO_4·7H_2O$), Concentrated hydrochloric acid (HCl, 37%) and ethanol were provided by Sinopharm Chemical Reagent Co. Ltd. (Shanghai, China). Ti_3AlC_2 power (400 mesh) was purchased from 11 Technology Co., Ltd (China). Sodium stannate trihydrate ($Na_2SnO_6·3H_2O$) and lithium fluoride (LiF) were supplied from

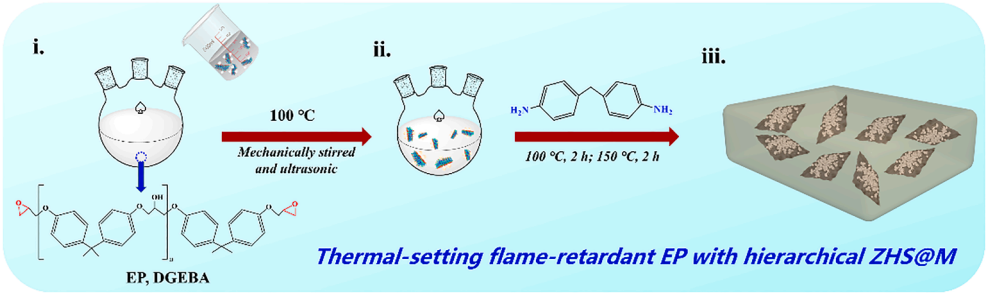

Fig. 2. Scheme route of fire safe EP-ZHS@M composites.

the Aladdin Reagent Co. Ltd., China. Bisphenol-A type Epoxy resin (EP, DGEBA type) was provided from Shixian Chemical Industry Co., Ltd. 4,4′-Diaminodiphenyl methane (DDM) and acetone were obtained from Sinopharm Chemical Reagent Co., Ltd.

2.2. Construction of hierarchical structure ZHS@M

The zinc hydroxystannate@$Ti_3C_2T_x$ (ZHS@M) hierarchical nanocomposite was prepared *via* a facile in-situ growth approach. Firstly, the 2D $Ti_3C_2T_x$ MXene suspension was diluted into 1.00 mg/mL, 280 mL. Then 1 mmol $ZnSO_4{\cdot}7H_2O$ was dissolved into the above MXene dispersion and kept magnetically stirred for 30 min. After that, $Na_2SnO_6{\cdot}3H_2O$ (1 mmol, 50 mL in distilled water) was added slowly dropwise in the Zn^{2+}-MXene dispersion within 1 h and the reaction kept conducting for the next 6 h at ambient temperature. Finally, the hierarchical structure of ZHS@M was obtained after 3 time washing and dried at 50 ℃ in vacuum oven overnight (Fig. 1).

2.3. Preparation of EP-ZHS@M composites

The Epoxy composites (EP-ZHS@M) was prepared by the two-step curing method. Typically, 0.5 wt%, 1.0 wt%, and 2.0 wt% ZHS@M was thoroughly dispersed in certain amount of acetone, respectively. Then 50 g EP was poured into the above dispersion and kept stirred and ultrasonic for 1 h. After that, the EP-ZHS@M mixture was heated to 100 ℃ to remove the acetone. And then 10.89 g DDM was rapidly added into the well-distributed mixture and pre-curing for 4 min at 100 ℃. After the pre-curing procedure, the mixture was poured into a mold for 2 h curing at 100 ℃ and then 150 ℃ for another 2 h. At last, the EP-ZHS@M with different amount of hierarchical 0D-2D nanocomposites were prepared (recorded as EP-0.5/1.0/2.0 ZHS@M). Notedly, the blank EP, EP-2.0 M, and EP-2.0 ZHS were also prepared in the same method (Fig. 2).

3. Results and discussions

3.1. Morphology and structure

The preparation route of delaminated $Ti_3C_2T_x$ was shown in Fig. 1 **(a)**. And the morphology and microstructure of delaminated $Ti_3C_2T_x$ nanosheets are characterized in **Fig. S3(d-f)**. After etching the Al phase layers, the flurry exhibited accordion-like multilayered shape. After ultrasonic treatment, the delaminated $Ti_3C_2T_x$ nanosheets are obtained, and the SEM image displays that $Ti_3C_2T_x$ exhibited nanosheets appearance, which indicated the Al atoms were successfully removed after etching. TEM image also provides further insight into the surface structural details. As observed in **Fig. S3**, $Ti_3C_2T_x$ shows as clear ultrathin nanosheet with typical 2D layered structure and transparent feature, which becomes soft and slightly wrinkled. As for ZHS, **Fig. S3(a-c)** exhibited their cube-like appearance and the diameter of these nanocubes were ~104 nm[18,19].

To learn more details about the structure of $Ti_3C_2T_x$, X-ray diffraction (XRD) was used to investigate the bulk Ti_3AlC_2 and delaminated $Ti_3C_2T_x$. The XRD results are presented in Fig. 3**a**. Comparing with the results before and after exfoliation, the main peak at $2\theta = \sim 39°$ assigned to the (104) plane of Ti_3AlC_2, is replaced by a broadened peak with a lower intensity, suggesting the Al-layers are selectively etched from the raw material[20,21]. The main (002) peak is shifted to a lower angle, indicating a loss of correlation between the layers and a larger interlayer

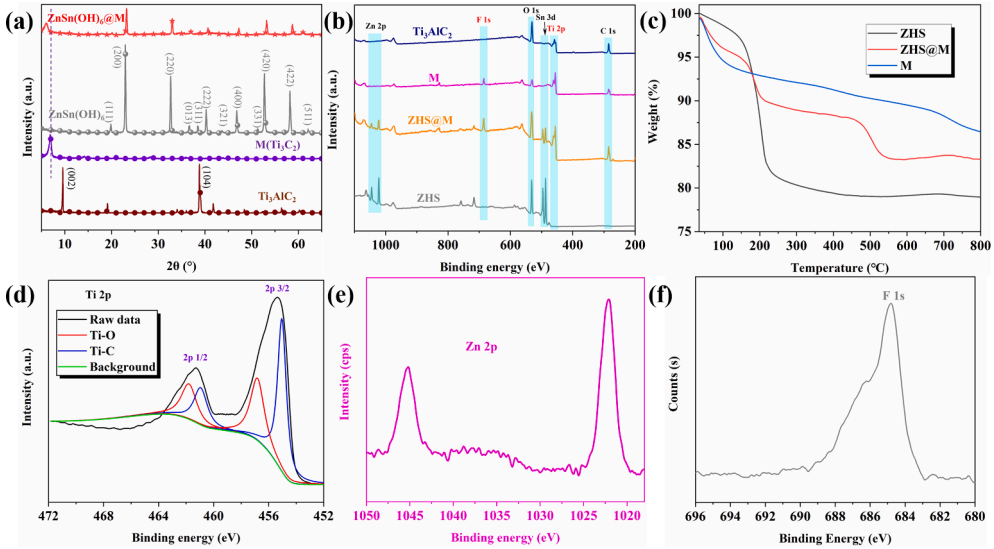

Fig. 3. (a) XRD patterns of Ti_3AlC_2, $Ti_3C_2T_x$, ZHS, and ZHS@M; (b) XPS spectra of Ti_3AlC_2, $Ti_3C_2T_x$, ZHS, and ZHS@M; (c) TGA curves of ZHS, M, ZHS@M under air atmosphere; (d-f) high resolution XPS spectra of Ti 2p, Zn 2p, and F 1 s from ZHS@M.

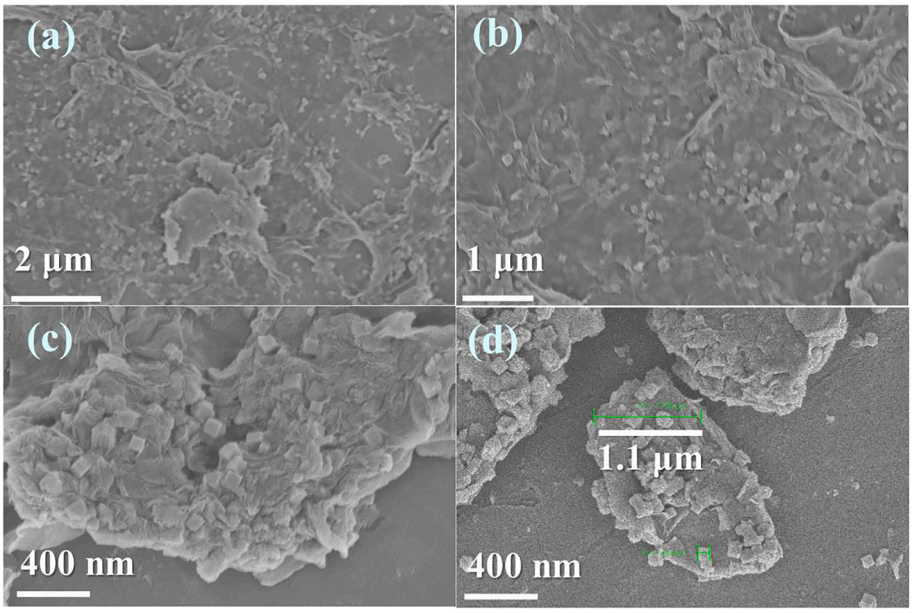

Fig. 4. (a–d) SEM images of 0D-2D hierarchical structure of ZHS@M.

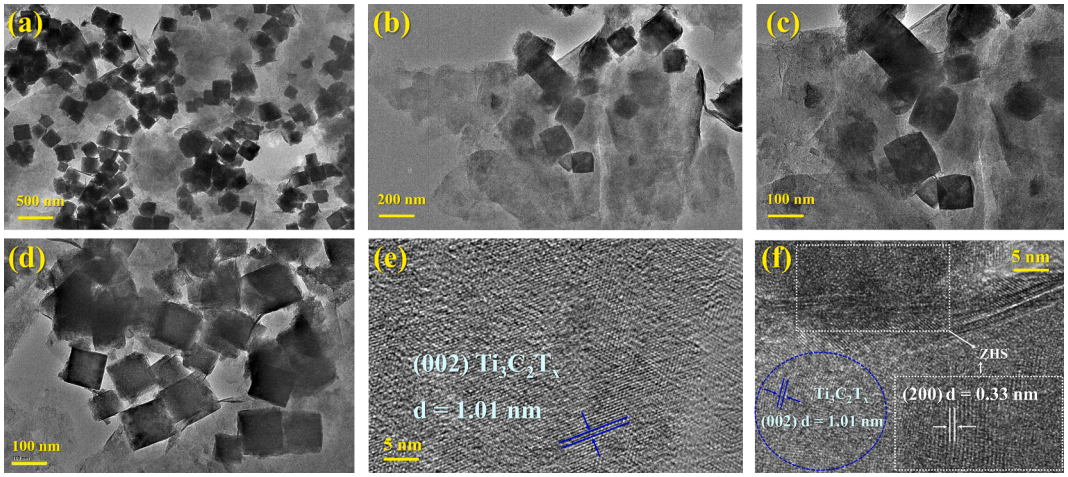

Fig. 5. (a–d) TEM images of 0D-2D hierarchical structure of ZHS@M, (e) HRTEM image of Ti3C2Tx, (f) HRTEM image of ZHS@M.

distance in c-lattice parameter.

Moreover, the X-ray photoelectron spectroscopy (XPS) results (Fig. 2**c**) also suggested that the Al is selectively etched from the Ti_3AlC_2 by tracing the Li 1 s and F 1 s at around 60.5 and 685.0 eV. In addition, such mild etching method usually begins from the outside of Ti_3AlC_2 and slightly moves forward into the inner Al layers. As a result, this method possesses exposed Ti atoms and then forming C—C and C-Ti bonds. Thus, the superior C content could be explained from MXene. Notedly, the appearance of O and F could be attributed to the formation of functional groups (═O, —F, OH) on the $Ti_3C_2T_x$ nanosheets surface, which further demonstrated the excellent being modified or potentially exceeding interacted capacity. In Fig. 3**d**, two peaks coming from Ti were obviously enhanced and obviously sliced to higher binding energy after etching reaction. This is because of the electrophilic interaction and the polarization of the vivo groups. And in **Fig. S5**, the high resolution of C 1 s was presented, the C-Ti bonds and C—C bonds could be seen at 281.2 eV and 284.6 eV, respectively. Furthermore, the C-O (286.4 eV) and O—C═O (288.9 eV) bonds proved the rich surface groups of the MXene nanosheets[14,22].

In Fig. 3**(a)**, all of the main characteristic diffraction peaks were well indexed to primitive standard cubic phase ZHS with the perovskite structure (JCPDS: NO. 74-1825), indicating the high purity of the ZHS [16]. Furthermore, the XPS result of ZHS showed up obvious Zn 2p peak and Sn 3d peak at 1020–1050 eV and ~500 eV, respectively. In addition, the hierarchical ZHS@M showed up similar peak at XRD compared with ZHS and the (002) performed lower angle compared with the pure MXene[15]. Furthermore, Fig. 3**(c)** exhibited thermal stability of ZHS, M, and ZHS@M under air atmosphere, and there was apparent two-step for the decomposition of ZHS and ZHS@M. What's more, after constructing the nanocubic ZHS on $Ti_3C_2T_x$ nanoflakes, the thermal stability of ZHS@M was improved compared with the ZHS, indicating as promising nanofiller for enhancing the fire safety for polymer matrix.

Fig. 1**(b and c)** demonstrated the preparation of hierarchical ZHS@M. As observed in Figs. 4 and 5, the SEM and TEM images presented well-distributed ZHS nanocubes on MXene nanosheets. Interestingly, after the *in-situ* construction of hierarchical structure, the diameter of ZHS did not exhibited large change and still maintain 100 nm or so, demonstrating this high stability of ZHS@M nanohybrid.

As presented in Fig. 2, the EP-ZHS@M composites were prepared *via* two-step method. At first, the ZHS@M nanomaterials were dispersed in

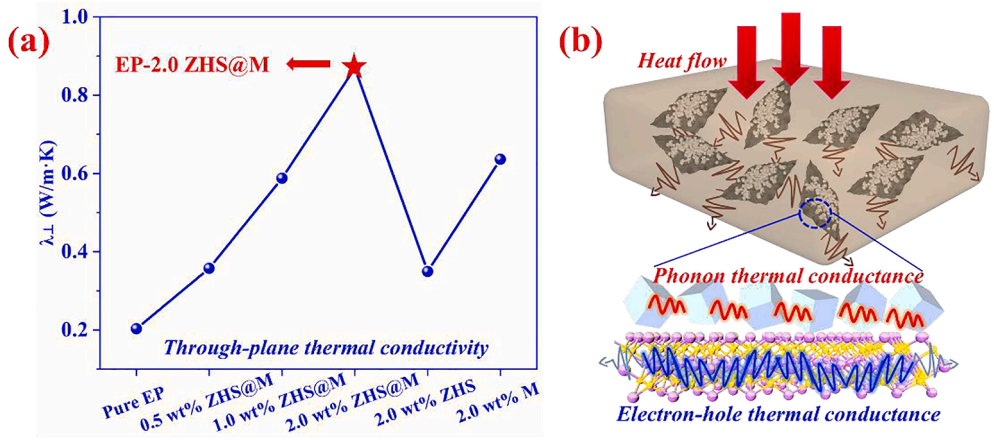

Fig. 6. (a) The through-plane thermal conductivity of EP and its ZHS@M composites; (b) the mechanism of enhanced conductance behavior.

DGEBA to obtain the highly homogenous pre-polymer. After that the DDM was poured into the above suspension and first stage was cured at 100 ℃ for 2 h. Then the second step was further cured at 150 ℃ for 2 h. As a result, the hierarchical ZHS@M was well-distributed in the EP and the thermo-setting EP-ZHS@M composites were successfully synthesized. Apparently, the labyrinth route (Fig. S4) was constructed with the help of $Ti_3C_2T_x$ nanosheets, indicating the barrier among the EP matrix.

3.2. Thermal conductance

Thermal conductivity (TC) is considered as one of the most vital factors for the applications in the thermal management[2–4]. With the increasing development of modern electronics and devices, the unavoidable heat release should need to be dissipated in time. In general, EP was a typical advanced polymer package material in thermal management due to excellent electrical and thermal property. The thermal conductivity, however, of the neat EP exhibited poor applied potential. Thus, it is a vital that develop a facile and efficient method to improve the thermal conductivity of EP.

As shown in Fig. 6**(a)** and Table S5, the neat EP showed up only 0.2031 W/m·K, and with the increasing amount of ZHS@M, the TC of these composites gradually enhanced up to 0.8691 W/m·K. After adding 2.0 wt% ZHS, EP-2.0 ZHS still performed poor thermal management capacity though the high crystalline ZHS endowed the exceeding phonon thermal conductance. This is because the low addition for the EP, which is not capable for constructing the thermal conductive network. Moreover, EP-2.0 M exhibited exceeding enhancement on thermal conductivity compared with pure EP, owing to the large specific area and electron-hole pair for the heat delivery. Besides, the surface groups of MXene can make the ZHS@M interact tightly with the EP matrix due to the hydrogen bonds, which showing benefit to improve the thermal conductivity. Most interestingly, the hierarchical ZHS@M nanofiller offered the extraordinary TC for EP composites, and EP-2.0 ZHS@M presented 0.8691 W/m·K TC. Thanks to the synergetic effect between ZHS and $Ti_3C_2T_x$, the TC of EP was enhanced by 328%.

To further investigated the thermal management mechanism, the potential diagram was shown in Fig. 6**(b)**. First, the heat flow reached the surface of EP composite and soon entered into the inner matrix. With the help of ZHS@M, the heat was rapidly delivered and passed away. During this process, the electron-hole thermal conductance played an essential role to conduct the heat, bridging the thermal conductive network with ZHS[6,23]. In addition, the phonon thermal conductance from ZHS was connected by the $Ti_3C_2T_x$ nanosheets, too. As a result, EP-ZHS@M composites constructed electron-hole bridged hierarchical phonon thermal conductance mechanism to enhance the thermal management capacity[5,24,25]. Therefore, these EP-ZHS@M composites not only performed excellent fire safety and smoke suppression capacity, but also showed exceedingly enhanced thermal conductivity, which was of great benefit for heat radiation of the modern electronic products.

3.3. Thermal stability

As presented in thermogravimetric analysis (TGA) and differential thermogravimetric analysis (DTG) curves (Fig. 7), the thermal stability of these EP composites exhibited similar tendency and more detailed data could be found in Tables S2 and S3. In Fig. 7**(a and b)**, the initial decomposition temperature ($T_{5\ wt\%}$) of these EP composites under N_2 atmosphere ranged from 351 ℃ to 372 ℃. Furthermore, there were obvious one stage during the decomposition of EP composites observed from the DTG curves. This is mainly attributed to the decomposition of

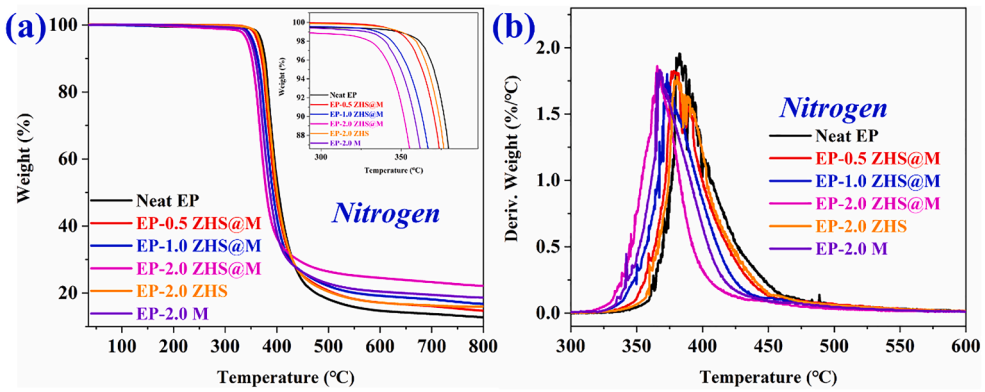

Fig. 7. (a and b) TGA and DTG curves from these EP composites under N_2 atmosphere, respectively.

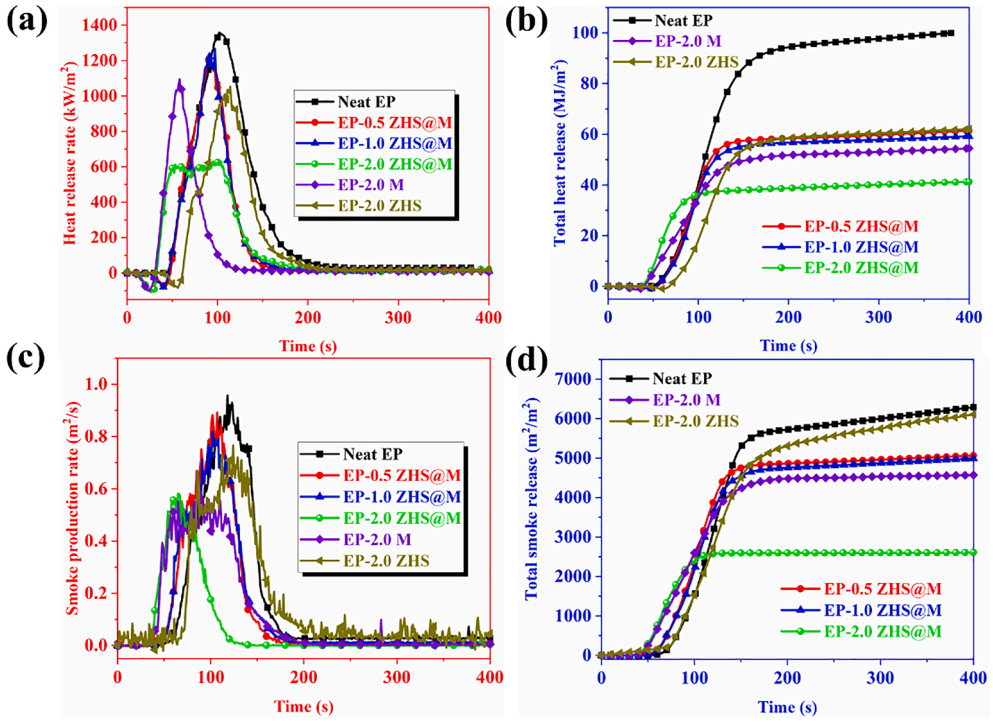

Fig. 8. The combustion behavior of neat EP and EP-ZHS@M composites: (a) HRR curves; (b) THR curves; (c) SPR patterns; (d) TSR curves.

the macromolecular chains of DGEBA[26]. With the incorporation of ZHS@M nanofillers, the thermal stabilities of the composites are all enhanced, showing an increasing residue (from 14.68% to 24.53%). However, the thermal stabilities of EP-2.0 ZHS@M and EP-2.0 M have been low down to 354.8 ℃ and 351.4 ℃. As for EP-2.0 ZHS@M, it can be concluded that the addition of ZHS promoted the pre-decomposition of EP composites due to the low decomposition temperature of ZHS. More importantly, the enhanced TC of these two EP composites easily lead the heat to be delivered into the inner part of polymeric materials [15,27,28]. As a result, $T_{5\ wt\%}$ became lower and this seemed to not benefit for the flame retardancy. However, the char residue of them raised by 67.10% and 39.31%, respectively, indicating the enhanced carbon-forming capacity during the combustion. Obviously, this evidence endowed the enhanced fire safety of EP owing to the self-cross-linking behavior in the high temperature[29,30]. Hierarchical structure of ZHS@M offered powerful radical quenching ability due to its large amount of defect. Moreover, the decomposition of ZHS@M into ternary metal oxide catalyzed the self-cross-linking behavior, which was vital to obtain more carbon char residues. Thereby, the exceeding carbon char residue offered better thermal insulating effect and implied the strengthened fire safety of EP composites when the thermal runaway of electronic products happened.

3.4. Fire safety

Cone calorimeter test, one of the most effective tools and directly methods, revealed the real flame retardant capacity of materials in a fire disaster [31,32]. Indeed, what a flame-retardant method does is mainly to earn more escape time and provide more safe time for people in a thermal runaway incident. Time to ignition (TTI) is usually adopted to evaluate the fire safe index of materials[33]. As presented in Fig. 8**(a** and **c)**, EP-2.0 ZHS@M showed up the shortest TTI, 36 s, due to the highest TC. But the heat release time and amount exhibited the lowest one, indicating low thermal disaster during thermal runaway-caused fire hazards. Furthermore, fire performance index (FPI), which is equal to the value of TTI/pHRR, is used to evaluate the fire performance when the materials facing a fire incident[34]. As expected, EP-2.0 ZHS@M performed a FPI of 0.057 s·m^2/kW, demonstrating a high fire safety. This is because the highest TC of EP-2.0 ZHS@M resulting the smallest TTI. What's more, the barrier effect or labyrinth structure accused the platform in HRR curve of EP-2.0 ZHS@M, which restricted the heat release in the thermal combustion. (Detailed values of *TTI, FPI could be found in supporting information*)

Furthermore, the particular results of heat release rate (HRR), peak heat release rate (pHRR) and total heat release (THR) from the samples were shown in Table S4 and the curves of HRR and THR are shown in Fig. 8**(a and b)**. As we can see, the ignition of these EP composites occurred earlier than neat EP due to the introduction of ZHS. According to the HRR patterns, neat EP burned dramatically and its HRR curve forms a sharply single peak with a pHRR value of 1358.79 kW/m^2. After introducing hierarchical ZHS@M nanomaterials, EP-2.0 ZHS@M showed a wider platform than that of pure EP with a sharp decrease to 629.41 kW/m^2, which only using with 2 wt% ZHS@M and accomplishing 54.91% abatement. Thus, ZHS@M hierarchical nanomaterial successfully tried their efforts to restrict the heat-releasing behavior of EP composites resulting in excellent fire safety.

What's more, the total heat release (THR) results show the similar trends with the above discussions. In particular, EP-2.0 ZHS@M (41.22 MJ/m^2) exhibited lowest THR values which reduced by 58.74% than that of pure EP (99.95 MJ/m^2). As mentioned above, ZHS@M were well-distributed in the matrix, which act as a barrier layer for the polymer matrix when facing a fire hazard. In general, the $Ti_3C_2T_x$ nanosheets acted as a barrier to prevent the meteoric heat from fire to damage the EP. Furthermore, the ZHS nanocubes possessed the fire safety due to their catalytic capacity of trapping free radical coming up from the combustion of EP. As a result, the labyrinth route built by MXene nanosheets and the free radical quenching ability from ZHS played an essential role for enhancing the fire safety[35,36]. More importantly, the integrated ZHS@M exhibited extraordinary synergetic effect without the disturb during the preparation.

Therefore, there was a conclusion that homogeneously dispersed ZHS@M nanocomposites made the positive role of reducing the heat release of EP and enhancing the fire safety with earning more escaping time for people in fire incidents when a thermal runaway happening.

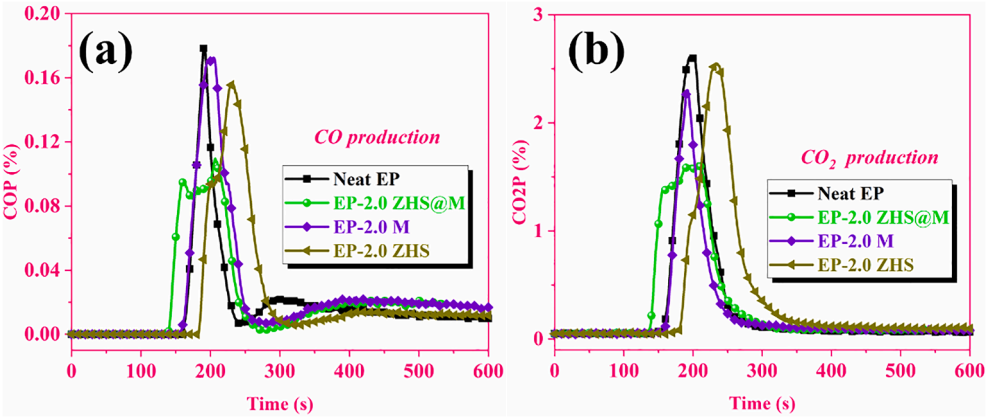

Fig. 9. The gases release from cone calorimeter of neat EP and EP-ZHS@M composites: (a) CO production; (b) CO_2 production.

Besides, ZHS@M also performed exceeding thermal management due to the 0D-2D hierarchical structure. This nanohybrid not only offered thermal conductor capacity, but also provided excellent precise for constructing labyrinth structure of EP for reducing fire risk.

In the past decades, researchers have figured out that toxicity release was one of the main killers whom lead to death in a fire incident, thus suppressing it would earn more evacuated time for people and reduce mortality in fire hazards[37,38]. Unfortunately, most of polymer materials including EP would release mortal smokes or gases during combustion. Therefore, smoke suppression is an urgent problem to be solved for the further applications of EP[31]. Fig. 8**(c and d)** performed the smoke production rate (SPR) and total smoke release (TSR) curves, respectively, during the combustion of EP, which are acquired from cone calorimeter. Expectedly, after using ZHS@M, both of the SPR and TSR were significantly decreased. Compared with pure EP, the indexes of TSR and peak SPR (pSPR) reduced 58.49% and 32.29% with 2 wt% content, respectively, indicating the outstanding capacity of ZHS@M nanomaterial on smoke reduction.

As mentioned above, the Ti element from the $Ti_3C_2T_x$ offered an efficient possibility for reducing the harmful gas from the combustion. The exceeding catalytic capacity endowed the reduction of SPR and TSR, providing excellent smoke suppression ability[39]. Moreover, the production of two typical hazardous gas, CO and CO_2, was dramatically decreased for this reason, too[30,36]. As shown in Fig. 9 and Table S5, the production of CO and CO_2 (named as COP and CO2P, respectively) were observed from CONE. According to results, COP of neat EP reached 0.18%, which did a great harm for human lives. Fortunately, the ZHS@M exhibited exceeding CO-release suppression capacity. EP-2.0 ZHS@M performed 0.10% yield in the same combustion situation, which reduced 44.44% compared with neat EP. Similarly, the issue of CO2P from the combustion of EP-2.0 ZHS@M exhibited highest decline among these EP composites. With 39.46% decrease compared with the neat one, this stifling gas was sharply reduced[7,40,41]. These results are attributed to the powerful catalytic capacity of ZHS@M. In detail, the transition metal carbide ($Ti_3C_2T_x$) offered intrinsic ability of reducing smoke, and the ZHS decomposed into ZnO and SnO when burning in a fire, which are also benefit to decrease the hazardous smoke [42]. As a result, ZHS@M turned into ZnO-SnO-TiO_2-$Ti_3C_2T_x$

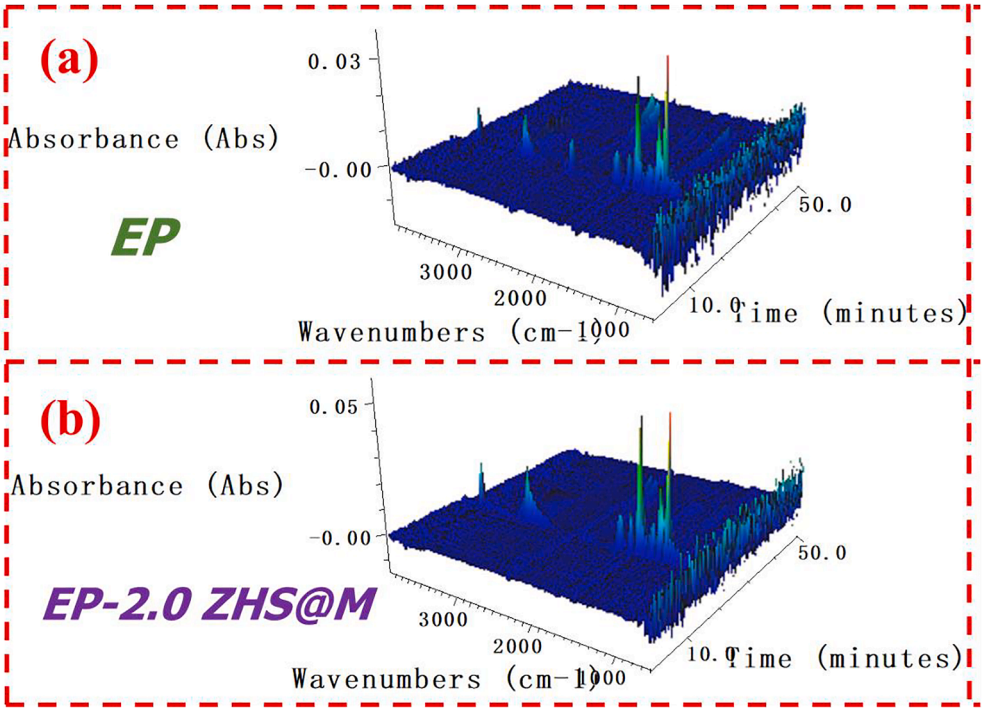

Fig. 10. 3D spectra of absorbance of the pyrolysis products from TG-IR test: (a) neat EP; (b) EP-2.0 ZHS@M.

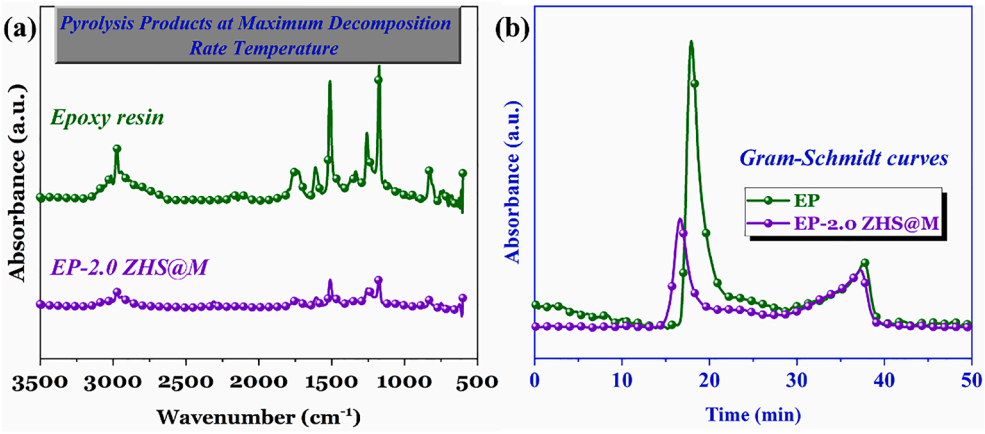

Fig. 11. (a) The absorbance at the maximum decomposition rate temperature (T_{max}); (b) Gram-Schmidt curves of EP and its composite.

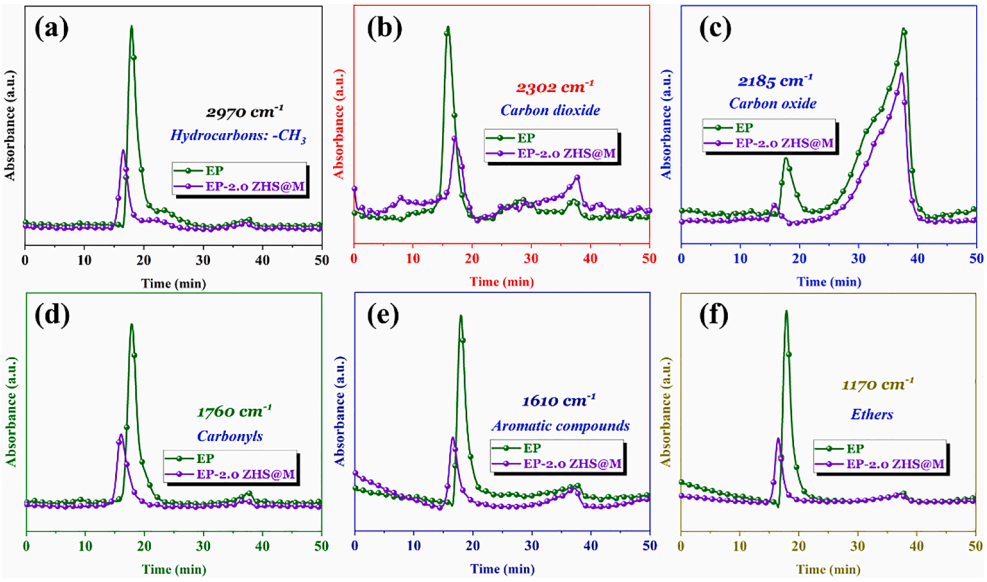

Fig. 12. Several typical hazardous pyrolyzed products absorption: (a) hydrocarbons; (b) CO_2; (c) CO; (d) carbonyls; (e) aromatic compounds; (f) ethers.

hierarchical ternary catalytic network. Therefore, ZHS@M nanocomposites possessed superior smoke suppression performance for cleaner EP, resulting outstanding flame safety in thermal runaway of electronic products.

3.5. Gas-phase evaluation

In order to further systematically understand the smoke suppression behavior of EP-2.0 ZHS@M composites, the pyrolysis products were systematically analyzed by thermogravimetric analysis-infrared spectrometry (TG-IR)[43]. Fig. 10**(a and b)** exhibit 3D absorbance images of EP and EP-2.0 ZHS@M, visually descripting the amounts of pyrolysis products. There was no apparent different peak between neat EP and EP-2.0 ZHS@M, implying the introduction of ZHS@M feebly affect the gaseous products in the thermal degradation procedure. As for the total absorbance of pyrolysis products from EP and EP-2.0 ZHS@M versus time (Fig. 11**(b)**, Gram-Schmidt curves) and FTIR spectra of pyrolysis gases at the maximum decomposition rate temperature (Fig. 11**(a)**), the peak intensity of EP-2.0 ZHS@M obviously reduced compared with pure EP, illustrating hierarchical ZHS@M possessed significant capacity on the pyrolysis gases generation of EP. Fig. 12**(a-f)** shows several characteristic peaks of several common hazardous pyrolysis products during decomposition of EP and EP-2.0 ZHS@M, including hydrocarbons (2980 cm^{-1}), CO_2 (2380 cm^{-1}), CO (2180 cm^{-1}), carbonyls (1743 cm^{-1}), aromatic compounds (1650 cm^{-1}), ethers (1110 cm^{-1}) [17,38].

Generally, CO are considered as the most dangerous volatile gases in the fire hazards[34]. The lower release of this pyrolysis hazardous compounds (PHCs) compared to the neat EP was significant to reduce the flame hazards and smoke toxicity in order to save people lives during a fire. Additionally, the other carcinogens such as carbonyls and ethers were also reduced. In addition, the lower releasement of hydrocarbons was benefit to stop the fire spread and expansion because the organic molecular was inflammable[44]. And this result also supported the low heat release of EP-2.0 ZHS@M mentioned above. Interestingly, CO_2, a noncombustible gas, fell into a decline, too. However, this phenomenon was supposed to a useful evidence that it reduced the risk of suffocating to death during a fire happening. From these TG-IR tests, we can conclude the ZHS@M could reduce the production of hazardous gases and smokes for enhancing smoke suppression behavior of EP. The low CO release was vital for human life during the fire hazards and the low CO_2 production made a great difference to prevent the death from asphyxia. Therefore, the low toxicity release and weaken heat deliver of the EP-based materials at its combustion behavior have proven that it accomplished the potential to be used as a safer polymer material facing thermal runaway.

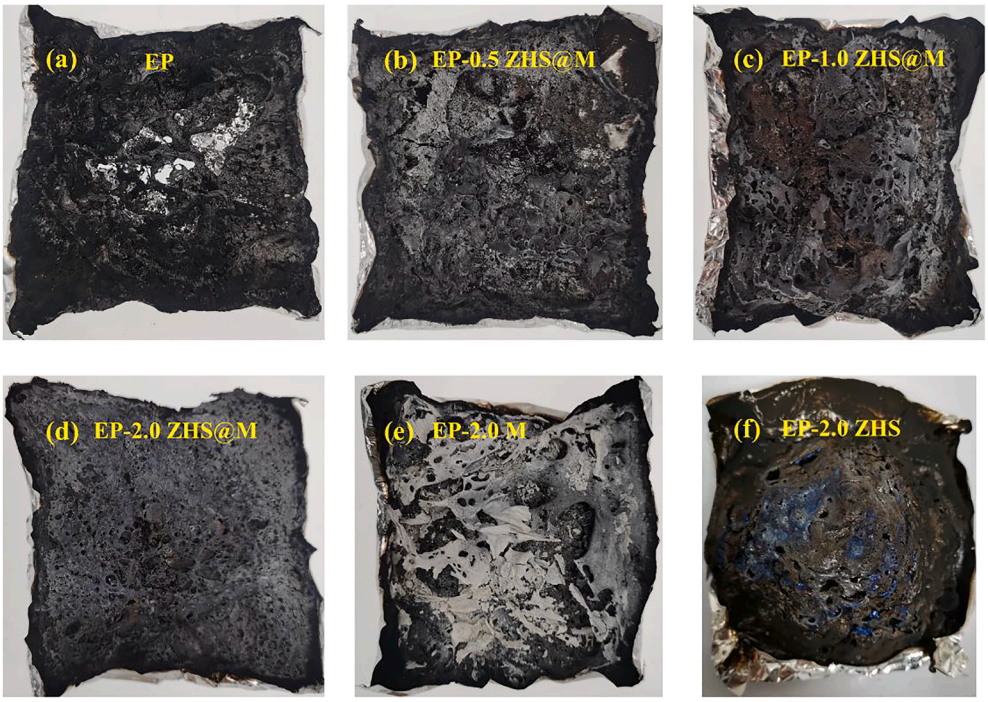

Fig. 13. Digital photographs of the char residue from EP and their composites after combustion: (a) neat EP; (b) EP-0.5 ZHS@M; (c) EP-1.0 ZHS@M; (d) EP-2.0 ZHS@M; (e) EP-2.0 M; (f) EP-2.0 ZHS.

3.6. Flame retardant mechanism

To better investigate the burning behavior, the digital photographs of char residues from the samples after cone calorimeter test are presented in Fig. 13. As can be seen in those digital photos, EP burns out with a little char residue. When adding 0.5 wt% ZHS@M, very few loose char residues are left and the appearance hard to remain a boxed shape. However, with the usage of 2.0 wt% ZHS@M, the appearance of residue became regular and the color changed into light white. This is partly because the oxidation of $Ti_3C_2T_x$ and transformation into TiO_2. Besides, when the combustion occurred, ZHS began to decomposed and transformed into zinc oxide (ZnO) and stannous oxide (SnO), which enhanced the catalytic effect[8,45,46]. Typically, the 2D $Ti_3C_2T_x$ nanosheets played as a role of protective barrier and gradually became TiO_2, which finally resulted a hierarchical structure ($Ti_3C_2T_x$-TiO_2-ZnO-SnO) protective layer to avoid the fire or heat spreading[47]. What's more, TiO_2-ZnO-SnO ternary catalytic capacity was attributed to the excellent smoke suppression behavior, too. Therefore, the decrease of heat and toxicity for EP composites is reasonable and expected.

To our knowledge, a rich and dense char layer can be regarded as a powerful shield to stop the transfer of flammable volatile and heat with advantage. However, the effectiveness of a protective layer is depended

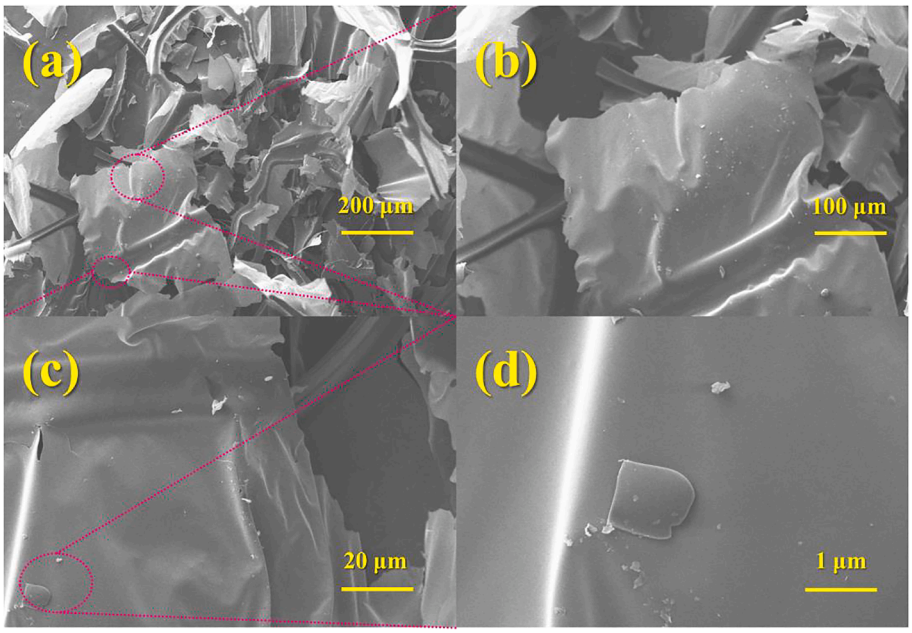

Fig. 14. (a–d) SEM images of the char residue from EP-2.0 ZHS@M.

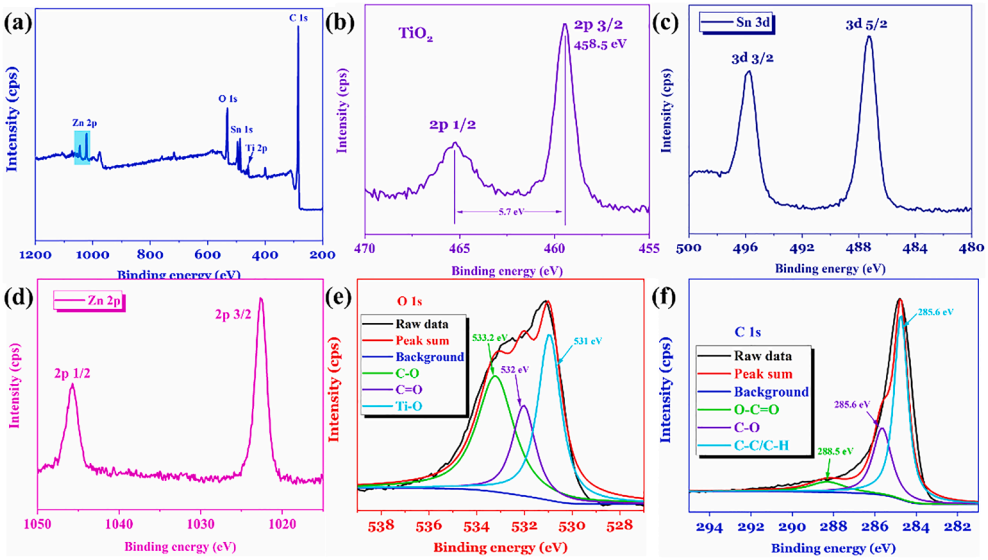

Fig. 15. (a) XPS spectrum of char residue from EP-2.0 ZHS@M, and its high resolution XPS spectra: (b) Ti 2p; (c) Sn 3d; (d) Zn 2p; (e) O 1 s; (f) C 1 s.

on the char-forming capacity[43,48]. Therefore, Raman spectra were adopted to further study the graphitic structure of char residues shown in **Fig. S2**. There exist two remarkable peaks at 1360 and 1590 cm^{-1} or so in all curves, which is belong to D band and G band. The ratio of the integrated area of D to G band in the testing range (I_D/I_G) is usually employed to determine the degree of graphic structure. Typically, the lower ratio of I_D/I_G, the higher graphitization degree of char is. And this result tends to offer more effectively protection of materials from burning procedure[49,50]. In these Raman spectra, the values of I_D/I_G obey the subsequence of EP-2.0 ZHS@M (2.15) < EP-2.0 M (2.31) < EP-2.0 ZHS (2.32) < EP (2.35). Obviously, it can be discovered that neat EP exhibited the highest I_D/I_G value which indicated the lowest graphitization degree. On the contrary, the EP-2.0 ZHS@M performed the exceeding graphitization degree. So, it is clear that why apparent attenuation of combustion and low heat deliver for EP-2.0 ZHS@M. In total, it can be said that ZHS@M nanocomposites catalyzed forming graphitized char layers with excellent capacity to protect the polymer matrix, thus enhancing the fire safety.

Furthermore, the components of the char residues are also vital to be learnt. In Fig. 14, the SEM images exhibited the char residue from EP-2.0 ZHS@M. These results indicated ZHS@M protector still remain nanosheet shape on the surface due to the migration of $Ti_3C_2T_x$-TiO_2-ZnO-SnO hierarchical structure after the burning process. In **Fig. S1**, the XRD patterns were shown and we could find that there is rutile TiO_2 in these samples. Furthermore, ZnO and SnO could be found in 25° and 36.5°, respectively. Thus, the $Ti_3C_2T_x$ nanosheets have been proven that they were transformed into TiO_2, and ZHS was changed into ZnO and SnO, indicating the ternary catalytic effect. As discussed above, we can know that the toxicity from gas phase was reduced[29,51]. Therefore, we can conclude that the flame-retardant mechanism of this phenomenon is attributed to the condensed phase char forming capacity and the reduction of flammable pyrolysis products from gas phase (diagram can be seen in Fig. 16). Overall, the enhanced char forming ability and toxicity suppression capacity offer superior fire safety for EP.

In addition, the components of the char residues are also carefully investigated by XPS[52]. As presented in Fig. 15**(a-d)**, there were apparent Ti, Zn and Sn-based component in the char residue. Furthermore, Fig. 15**(e and f)** determined the main component of this residue from EP-2.0 ZHS@M. As the C 1 s spectrum shown, the binding energies for C—C/C—H, C-O, and O—C═O were found at 284.7, 286.3, 288.2 eV, respectively. With the help of O 1 s spectrum, we can learn that the Ti-O, C-O, and C═O from 531 eV, 532 eV, and 533.2 eV, respectively, indicating the ternary metal oxide catalytic effect. Hence, from SEM, XRD, and XPS, we can thoroughly understand the flame retardant mechanism.

Therefore, these results from XRD, SEM and XPS ulteriorly demonstrated the exceeding fire safety and cleaner smoke release of EP and the flame retardant mechanism from condensed phase (Fig. 16). In short, the exceptional catalytic effect and barrier effect from ZHS@M nanomaterial effectively improved the fire safety and smoke suppression capacity, indicating a cleaner and safer production for the modern electronic applications for EP.

Fig. 16. The flame retardant mechanism of hierarchical ZHS@M: labyrinth effect and ternary catalytic effect.

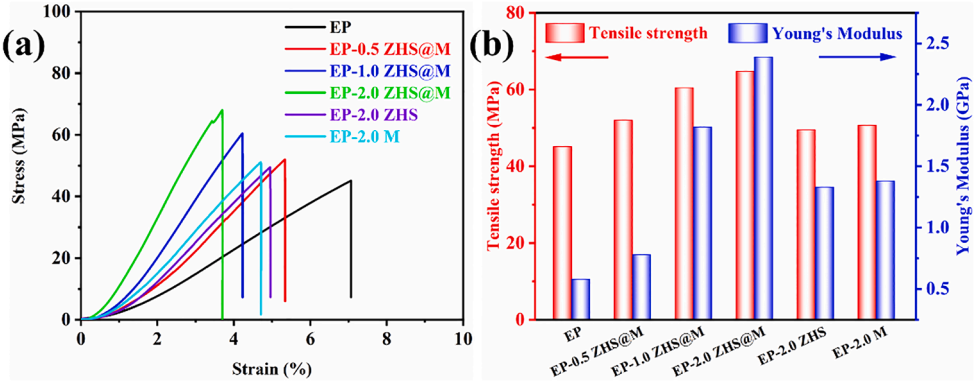

Fig. 17. (a) Stress-strain curves of EP and its ZHS@M composites; (b) the tensile property and modulus.

3.7. Mechanical performance

Generally, EP is one kind of advanced polymer with superior tensile strength and mechanical property must not be neglected during the practical applications[9]. As presented in Fig. 17**(a)** and Table S6, there were typical stress-strain curves for thermo-setting resin. In detail, the neat EP showed up 45.14 MPa tensile strength and 0.58 GPa modulus. EP-2.0 ZHS@M accomplished superior robustness of 64.71 MPa and Young's modulus of 2.39 GPa. Firstly, the ZHS@M nanohybrids generate strong hydrogen bonding interaction with epoxy resin molecular chain. The hydrogen bonds tightly connected with the molecular chain, resulting enhanced tensile strength. Secondly, the 0D-2D hierarchical ZHS@M are well-distributed in EP matrix, and these robust nano-networks construct the improvement of the mechanical property. These results exhibited the EP-ZHS@M still maintained the superior mechanical performance. Furthermore, there is a synergetic effect of ZHS@M for enhancing the mechanical strength as demonstrated in Fig. 17**(b)**. The robust $Ti_3C_2T_x$ nanosheets and high crystalline ZHS make the effort for the improved modulus and strength, indicating the superior mechanical performance for the electronic package materials.

4. Conclusion

As discussed above, a series of EP composites with outstanding thermal management capacity and fire safety were successfully prepared. The 0D-2D hierarchical structure of ZHS@M was obtained via a facile and efficient *in-situ* growth approach, and this hierarchical nanomaterial acted a vital factor for reducing fire risk. In particular, the ZHS@M not only offered improved the thermal conductivity via hierarchical thermal conductance approach, but also strengthened the flame retardancy of EP. In detail, the thermal conductivity was up to 0.8691 W/m·K due to the electron-hole bridged phonon thermal conductance mechanism, indicating the exceeding thermal management capacity. Furthermore, the pHRR and THR was efficiently reduced by more than 50% thanks to the hierarchical labyrinth structure. Interestingly, the CO and CO_2 production were decreased by 44.44% and 39.46% due to the ternary catalytic effect, respectively, when using 2 wt% ZHS@M. In addition, these EP-2.0 ZHS@M composite still remained superior mechanical robust of 64 MPa and high modulus of 2.39 GPa. Therefore, this work provided a facile and efficient method for solving thermal management in applications of modern electronic products and offered an efficient flame retardant EP composites when facing fire risks raised by thermal runaway.

Declaration of Competing Interest

The authors declare that they have no known competing financial interests or personal relationships that could have appeared to influence the work reported in this paper.

Acknowledgements

This work was supported by the National Natural Science Foundation of China (Nos. U1833113 and 51874266); and the Fundamental Research Funds for the Central Universities (Nos. WK2320000054 and WK2320000044).

Appendix A. Supplementary data

Supplementary data to this article can be found online at https://doi.org/10.1016/j.cej.2021.132046.

References

[1] W. Xia, X. Fei, Q. Wang, Y. Lu, M.T. Innocent, J. Zhou, S. Yu, H. Xiang, M. Zhu, Nano-hybridized form-stable ester@F-SiO2 phase change materials for melt-spun PA6 fibers engineered towards smart thermal management fabrics, Chem. Eng. J. 403 (2021) 126369, https://doi.org/10.1016/j.cej.2020.126369.
[2] L. Zhang, Q. Wei, J. An, L.i. Ma, K. Zhou, W. Ye, Z. Yu, X. Gan, C.-T. Lin, J. Luo, Construction of 3D interconnected diamond networks in Al-matrix composite for high-efficiency thermal management, Chem. Eng. J. 380 (2020) 122551, https://doi.org/10.1016/j.cej.2019.122551.
[3] X. Shen, F. Wang, Z. Mao, H. Xu, B. Wang, X. Sui, X. Feng, Biphasic organohydrogels based on phase change materials with excellent thermostability for thermal management applications, Chem. Eng. J. 416 (2021) 129181, https://doi.org/10.1016/j.cej.2021.129181.
[4] B. Shin, S. Mondal, M. Lee, S. Kim, Y.-I. Huh, C. Nah, Flexible thermoplastic polyurethane-carbon nanotube composites for electromagnetic interference shielding and thermal management, Chem. Eng. J. 418 (2021) 129282, https://doi.org/10.1016/j.cej.2021.129282.
[5] K. Wu, D. Liu, C. Lei, S. Xue, Q. Fu, Is filler orientation always good for thermal management performance: A visualized study from experimental results to simulative analysis, Chem. Eng. J. 394 (2020) 124929, https://doi.org/10.1016/j.cej.2020.124929.
[6] Y. Zhan, B. Nan, Y. Liu, E. Jiao, J. Shi, M. Lu, K. Wu, Multifunctional cellulose-based fireproof thermal conductive nanocomposite films assembled by in-situ grown SiO2 nanoparticle onto MXene, Chem. Eng. J. 421 (2021) 129733, https://doi.org/10.1016/j.cej.2021.129733.
[7] F. Karaer Özmen, M.E. Üreyen, A.S. Koparal, Cleaner production of flame-retardant-glass reinforced epoxy resin composite for aviation and reducing smoke toxicity, Journal of Cleaner Production 276 276 (2020) 124065, https://doi.org/10.1016/j.jclepro.2020.124065.
[8] F. Carosio, L. Maddalena, J. Gomez, G. Saracco, A. Fina, Graphene Oxide Exoskeleton to Produce Self-Extinguishing, Nonignitable, and Flame Resistant Flexible Foams: A Mechanically Tough Alternative to Inorganic Aerogels, Adv. Mater. Interfaces 5 (23) (2018) 1801288, https://doi.org/10.1002/admi.v5.2310.1002/admi.201801288.
[9] Z. Qu, C.-a. Xu, Z. Hu, Y. Li, H. Meng, Z. Tan, J. Shi, K. Wu, (CF3SO3)3Er-decorated black phosphorene for robust ambient stability and excellent flame retardancy in epoxy resin, Composites Part B: Engineering 202 (2020) 108440, https://doi.org/10.1016/j.compositesb:2020.108440.
[10] F. Chu, Z. Xu, Y. Zhou, S. Zhang, X. Mu, J. Wang, W. Hu, L. Song, Hierarchical core–shell TiO2@LDH@Ni(OH)2 architecture with regularly-oriented nanocatalyst shells: Towards improving the mechanical performance, flame retardancy and toxic smoke suppression of unsaturated polyester resin, Chem. Eng. J. 405 (2021).
[11] B. Liu, Y. Li, T. Fei, S. Han, C. Xia, Z. Shan, J. Jiang, Highly thermally conductive polystyrene/polypropylene/boron nitride composites with 3D segregated structure prepared by solution-mixing and hot-pressing method, Chem. Eng. J. 385 (2020) 123829, https://doi.org/10.1016/j.cej.2019.123829.

[12] M. Naguib, M. Kurtoglu, V. Presser, J. Lu, J. Niu, M. Heon, L. Hultman, Y. Gogotsi, M.W. Barsoum, Two-dimensional nanocrystals produced by exfoliation of Ti3 AlC2, Adv Mater 23 (37) (2011) 4248–4253.

[13] M. Naguib, V.N. Mochalin, M.W. Barsoum, Y. Gogotsi, 25th anniversary article: MXenes: a new family of two-dimensional materials, Adv Mater 26 (2014) 992–1005.

[14] F. Shahzad, M. Alhabeb, C.B. Hatter, B. Anasori, S. Man Hong, C.M. Koo, Y. Gogotsi, Babak Anasori, Soon Man Hong, Chong Min Koo, Yury Gogotsi, Electromagnetic interference shielding with 2D transition metal carbides (MXenes), Science 353 353 (6304) (2016) 1137–1140.

[15] B. Wang, H. Sheng, Y. Shi, L. Song, Y. Zhang, Y. Hu, W. Hu, The influence of zinc hydroxystannate on reducing toxic gases (CO, NO(x) and HCN) generation and fire hazards of thermoplastic polyurethane composites, J Hazard Mater 314 (2016) 260–269.

[16] W. Wang, Y. Kan, J. Liu, K.M. Liew, L. Liu, Y. Hu, Self-assembly of zinc hydroxystannate on amorphous hydrous TiO2 solid sphere for enhancing fire safety of epoxy resin, J Hazard Mater 340 (2017) 263–271.

[17] X. Zhou, S. Qiu, W. Xing, C.S.R. Gangireddy, Z. Gui, Y. Hu, Hierarchical Polyphosphazene@Molybdenum Disulfide Hybrid Structure for Enhancing the Flame Retardancy and Mechanical Property of Epoxy Resins, ACS Appl Mater Interfaces 9 (34) (2017) 29147–29156.

[18] J. Lu, Y. Zhang, Y. Tao, B. Wang, W. Cheng, G. Jie, L. Song, Y. Hu, Self-healable castor oil-based waterborne polyurethane/MXene film with outstanding electromagnetic interference shielding effectiveness and excellent shape memory performance, J Colloid Interface Sci 588 (2021) 164–174.

[19] W. Cheng, Y. Zhang, W. Tian, J. Liu, J. Lu, B. Wang, W. Xing, Y. Hu, Highly Efficient MXene-Coated Flame Retardant Cotton Fabric for Electromagnetic Interference Shielding, Ind. Eng. Chem. Res. 59 (31) (2020) 14025–14036.

[20] J.i. Liu, H.-B. Zhang, R. Sun, Y. Liu, Z. Liu, A. Zhou, Z.-Z. Yu, Hydrophobic, Flexible, and Lightweight MXene Foams for High-Performance Electromagnetic-Interference Shielding, Adv Mater 29 (38) (2017) 1702367, https://doi.org/10.1002/adma.201702367.

[21] P. Sambyal, A. Iqbal, J. Hong, H. Kim, M.-K. Kim, S.M. Hong, M. Han, Y. Gogotsi, C. M. Koo, Ultralight and Mechanically Robust Ti3C2Tx Hybrid Aerogel Reinforced by Carbon Nanotubes for Electromagnetic Interference Shielding, ACS Appl Mater Interfaces 11 (41) (2019) 38046–38054.

[22] Z. Fan, D. Wang, Y. Yuan, Y. Wang, Z. Cheng, Y. Liu, Z. Xie, A lightweight and conductive MXene/graphene hybrid foam for superior electromagnetic interference shielding, Chem. Eng. J. 381 (2020) 122696, https://doi.org/10.1016/j.cej.2019.122696.

[23] Y.i. Wang, Z. Cao, J. Wu, C. Ma, C. Qiu, Y. Zhao, F. Shao, H. Wang, J. Zheng, G. Huang, Mechanically robust, ultrastretchable and thermal conducting composite hydrogel and its biomedical applications, Chem. Eng. J. 360 (2019) 231–242.

[24] Y.u. Wang, W. Wang, R. Xu, M. Zhu, D. Yu, Flexible, durable and thermal conducting thiol-modified rGO-WPU/cotton fabric for robust electromagnetic interference shielding, Chem. Eng. J. 360 (2019) 817–828.

[25] K.V. Mahesh, V. Linsha, A. Peer Mohamed, S. Ananthakumar, Processing of 2D-MAXene nanostructures and design of high thermal conducting, rheo-controlled MAXene nanofluids as a potential nanocoolant, Chem. Eng. J. 297 (2016) 158–169.

[26] X. Fan, G. Zhang, Q. Gao, J. Li, Z. Shang, H. Zhang, Y.u. Zhang, X. Shi, J. Qin, Highly expansive, thermally insulating epoxy/Ag nanosheet composite foam for electromagnetic interference shielding, Chem. Eng. J. 372 (2019) 191–202.

[27] R. Xu, B. Deng, L. Min, H. Xu, S. Zhong, CuSn(OH)6 submicrospheres: Room-temperature synthesis and weak antiferromagnetic behavior, Mater. Lett. 65 (2011) 733–735.

[28] B. Wang, H. Sheng, Y. Shi, W. Hu, N. Hong, W. Zeng, H. Ge, X. Yu, L. Song, Y. Hu, Recent advances for microencapsulation of flame retardant, Polym. Degrad. Stab. 113 (2015) 96–109.

[29] P.-P. Zhao, C. Deng, Z.-Y. Zhao, S.-C. Huang, P. Lu, Y.-Z. Wang, Nanoflake-Constructed Supramolecular Hierarchical Porous Microspheres for Fire-Safety and Highly Efficient Thermal Energy Storage, ACS Appl Mater Interfaces 12 (25) (2020) 28700–28710.

[30] W. Rao, P. Zhao, C. Yu, H.-B. Zhao, Y.-Z. Wang, High strength, low flammability, and smoke suppression for epoxy thermoset enabled by a low-loading phosphorus-nitrogen-silicon compound, Compos. B Eng. 211 (2021) 108640, https://doi.org/10.1016/j.compositesb:2021.108640.

[31] Y. Sheng, Y. Wu, Y.u. Yan, H. Jia, Y. Qiao, B.S. Underwood, D. Niu, Y.R. Kim, Development of environmentally friendly flame retardant to achieve low flammability for asphalt binder used in tunnel pavements, J. Cleaner Prod. 257 (2020) 120487, https://doi.org/10.1016/j.jclepro.2020.120487.

[32] F. Carosio, G. Laufer, J. Alongi, G. Camino, J.C. Grunlan, Layer-by-layer assembly of silica-based flame retardant thin film on PET fabric, Polym. Degrad. Stab. 96 (5) (2011) 745–750.

[33] B. Wang, Q. Tang, N. Hong, L. Song, L. Wang, Y. Shi, Y. Hu, Effect of cellulose acetate butyrate microencapsulated ammonium polyphosphate on the flame retardancy, mechanical, electrical, and thermal properties of intumescent flame-retardant ethylene-vinyl acetate copolymer/microencapsulated ammonium polyphosphate/polyamide-6 blends, ACS Appl Mater Interfaces 3 (9) (2011) 3754–3761.

[34] Y. Shi, B. Yu, K. Zhou, R.K. Yuen, Z. Gui, Y. Hu, S. Jiang, Novel CuCo2O4/graphitic carbon nitride nanohybrids: Highly effective catalysts for reducing CO generation and fire hazards of thermoplastic polyurethane nanocomposites, J Hazard Mater 293 (2015) 87–96.

[35] W. Wang, Y. Pan, H. Pan, W. Yang, K.M. Liew, L. Song, Y. Hu, Synthesis and characterization of MnO2 nanosheets based multilayer coating and applications as a flame retardant for flexible polyurethane foam, Compos. Sci. Technol. 123 (2016) 212–221.

[36] L. He, J. Wang, B. Wang, X. Wang, X. Zhou, W. Cai, X. Mu, Y. Hou, Y. Hu, L. Song, Large-scale production of simultaneously exfoliated and Functionalized Mxenes as promising flame retardant for polyurethane, Composites Part B: Engineering 179 (2019) 107486, https://doi.org/10.1016/j.compositesb:2019.107486.

[37] Z. Wei, C. Cai, Y. Huang, P. Wang, J. Song, L. Deng, Y.u. Fu, Eco-friendly strategy to a dual-2D graphene-derived complex for poly (lactic acid) with exceptional smoke suppression and low CO2 production, J. Cleaner Prod. 280 (2021) 124433, https://doi.org/10.1016/j.jclepro.2020.124433.

[38] R. Panda, K.K. Pant, T. Bhaskar, S.N. Naik, Dissolution of brominated epoxy resin for environment friendly recovery of copper as cupric oxide nanoparticles from waste printed circuit boards using ammonium chloride roasting, Journal of Cleaner Production 291 (2021) 125928, https://doi.org/10.1016/j.jclepro.2021.125928.

[39] B. Yu, B. Tawiah, L.-Q. Wang, A.C. Yin Yuen, Z.-C. Zhang, L.-L. Shen, B.o. Lin, B. Fei, W. Yang, A.o. Li, S.-E. Zhu, E.-Z. Hu, H.-D. Lu, G.H. Yeoh, Interface decoration of exfoliated MXene ultra-thin nanosheets for fire and smoke suppressions of thermoplastic polyurethane elastomer, J Hazard Mater 374 (2019) 110–119.

[40] A.A. Wani, A.M. Khan, Y.K. Manea, M. Shahadat, S.Z. Ahammad, S.W. Ali, Graphene-supported organic-inorganic layered double hydroxides and their environmental applications: A review, J. Cleaner Prod. 273 (2020) 122980, https://doi.org/10.1016/j.jclepro.2020.122980.

[41] S. Lazar, F. Carosio, A.-L. Davesne, M. Jimenez, S. Bourbigot, J. Grunlan, Extreme Heat Shielding of Clay/Chitosan Nanobrick Wall on Flexible Foam, ACS Appl Mater Interfaces 10 (37) (2018) 31686–31696.

[42] X. Wang, T. Chen, C. Peng, J. Hong, Z. Lu, C. Yuan, B. Zeng, W. Luo, L. Dai, Synergistic Effect of Mesoporous Nanocomposites with Different Pore Sizes and Structures on Fire Safety and Smoke Suppression of Epoxy Resin, Macromol. Mater. Eng. 305 (2) (2020) 1900640, https://doi.org/10.1002/mame.v305.210.1002/mame.201900640.

[43] Y. Huang, S. Jiang, R. Liang, P. Sun, Y. Hai, L. Zhang, Thermal-triggered insulating fireproof layers: A novel fire-extinguishing MXene composites coating, Chem. Eng. J. 391 (2020) 123621, https://doi.org/10.1016/j.cej.2019.123621.

[44] S.-S. Chung, J.-S. Zheng, A.C.S. Kwong, V.W.Y. Lai, Harmful flame retardant found in electronic cigarette aerosol, J. Cleaner Prod. 171 (2018) 10–16.

[45] X.-W. Cheng, J.-P. Guan, X.-H. Yang, R.-C. Tang, F. Yao, A bio-resourced phytic acid/chitosan polyelectrolyte complex for the flame retardant treatment of wool fabric, J. Cleaner Prod. 223 (2019) 342–349.

[46] P. Sarath, M. Biswal, S. Mohanty, S.K. Nayak, Effect of silicone rubber based impact modifier on mechanical and flammability properties of plastics recovered from waste mobile phones, J. Cleaner Prod. 171 (2018) 209–219.

[47] P.-P. Zhao, C. Deng, Z.-Y. Zhao, P. Lu, S. He, Y.-Z. Wang, Hypophosphite tailored graphitized hierarchical porous biochar toward highly efficient solar thermal energy harvesting and stable Storage/Release, Chem. Eng. J. 420 (2021) 129942, https://doi.org/10.1016/j.cej.2021.129942.

[48] J. Wang, D. Zhang, Y. Zhang, W. Cai, C. Yao, Y. Hu, W. Hu, Construction of multifunctional boron nitride nanosheet towards reducing toxic volatiles (CO and HCN) generation and fire hazard of thermoplastic polyurethane, J Hazard Mater 362 (2019) 482–494.

[49] M. Mohsin, S.W. Ahmad, A. Khatri, B. Zahid, Performance enhancement of fire retardant finish with environment friendly bio cross-linker for cotton, J. Cleaner Prod. 51 (2013) 191–195.

[50] X.-X. Wang, J.-C. Shu, W.-Q. Cao, M. Zhang, J. Yuan, M.-S. Cao, Eco-mimetic nanoarchitecture for green EMI shielding, Chem. Eng. J. 369 (2019) 1068–1077.

[51] Y. Shi, C. Liu, Z. Duan, B. Yu, M. Liu, P. Song, Interface engineering of MXene towards super-tough and strong polymer nanocomposites with high ductility and excellent fire safety, Chem. Eng. J. 399 (2020) 125829, https://doi.org/10.1016/j.cej.2020.125829.

[52] W. Cai, W. Guo, Y. Pan, J. Wang, X. Mu, X. Feng, B. Yuan, B. Wang, Y. Hu, Polydopamine-bridged synthesis of ternary h-BN@PDA@SnO2 as nanoenhancers for flame retardant and smoke suppression of epoxy composites, Compos. A Appl. Sci. Manuf. 111 (2018) 94–105.